Infection and Drug Resistance

Dovepress
open access to scientific and medical research

Open Access Full Text Article

ORIGINAL RESEARCH

Molecular Mechanism of *Staphylococcus xylosus* Resistance Against Tylosin and Florfenicol

Mo Chen[1], Yanhua Li[1], Shu Li[2], Wenqiang Cui[2], Yonghui Zhou[3], Qianwei Qu[1], Ruixiang Che[4], Lu Li[5], Shuguang Yuan[2], Xin Liu[3]

[1]College of Veterinary Medicine, Northeast Agricultural University, Harbin, People's Republic of China; [2]Research Center for Computer-Aided Drug Discovery, Shenzhen Institutes of Advanced Technology, Shenzhen, People's Republic of China; [3]College of Basic Medicine, Guizhou University of Traditional Chinese Medicine, Guiyang, People's Republic of China; [4]College of Animal Science and Veterinary Medicine, Heilongjiang Bayi Agricultural University, Daqing, People's Republic of China; [5]College of Life Sciences, Northeast Agricultural University, Harbin, People's Republic of China

Correspondence: Shuguang Yuan, Research Center for Computer-Aided Drug Discovery, Shenzhen Institutes of Advanced Technology, Shenzhen, People's Republic of China, Tel +86-150-0209-0670, Email shuguang.yuan@siat.ac.cn; Xin Liu, College of Basic Medicine, Guizhou University of Traditional Chinese Medicine, Guiyang, People's Republic of China, Tel +86-188-8605-6643, Email 1046977102@qq.com

Purpose: Drug resistance presents an ever-increasing global public health threat that involves all major microbial pathogens and antimicrobial drugs. Strains that are resistant to multiple drugs pose severe clinical problems and cost lives. However, systematic studies on cross-resistance of *Staphylococcus xylosus* have been missing.

Methods: Here, we investigated various mutations in the sequence of ribosomal proteins involved in cross-resistance. To understand this effect on a molecular basis and to further elucidate the role of cross-resistance, we computationally constructed the 3D model of the large ribosomal subunit from *S. xylosus* as well as its complexes with both tylosin and florfenicol. Meanwhile, all-atom molecular dynamics simulations was used. In addition, the regulation of protein networks also played an essential role in the development of cross-resistance in *S. xylosus*.

Results: We discovered that the minimum inhibitory concentration against both tylosin and florfenicol of the mutant strain containing the insertion L22 97KRTSAIN98 changed dramatically. Further, we found that unique structural changes in the β-hairpin of L22 played a central role in this variant in the development of antibiotic resistance in *S. xylosus*. The regulation of protein networks also played an essential role in the development of cross-resistance in *S. xylosus*.

Conclusion: Our work provides insightful views into the mechanism of *S. xylosus* resistance that could be useful for the development of the next generation of antibiotics.

Keywords: antimicrobial resistance, *Staphylococcus xylosus*, cross-resistance evolution, ribosomal protein L22

Introduction

Antibiotic resistance occurs when bacteria or fungi develop the ability to defeat the drugs designed to kill them.[1] Worldwide, about 700,000 people die each year due to drug-resistant diseases, according to a report from the World Health Organization.[2,3] No one can completely avoid the risk of being affected by resistant infections. If antibiotics lose effectiveness, we lose the ability to treat serious infections and control public health.

Staphylococcus xylosus is a coagulase-negative, Gram-positive coccus that is widely distributed in the environment, as well as in the skin and mucosal surfaces of mammals.[4,5] *S. xylosus* is also naturally present in raw meat and milk, and in addition is used as a starter culture for manufacturing sausage, fermented cheese, and meat.[6] Although this strain is defined as an apparent nonpathogenic *Staphylococcus*, some strains unexpectedly were involved in bacterial infections in human and animal.[7,8] Therefore, ever-increasing attention is paid to the role *S. xylosus* plays in infectious diseases.

During the last few years, an increasing number of human infections have been associated with this species, such as urinary tract, pancreatic, cardiac, ophthalmologic, dental, bloodstream, erythema chest infections, and nodosum, as well as otogenic brain abscess.[8–11] Currently, *S. xylosus* has become the prevalent cause of mastitis in dairy herds in many countries, including the US, Finland, Canada, Sweden, Switzerland, Norway, and China.[12–15] The average proportion of

Received: 20 June 2022
Accepted: 16 September 2022
Published: 26 October 2022

mastitis due to *S. xylosus* increases year by year according to a nationwide survey.[13,16] *S. xylosus* can also lead to other diseases in animals, including dermatitis in gerbils and immunodeficient mice, pulmonary and lymph-node lesions in immunodeficient mice, or transmural necrotizing cystitis and secondary peritonitis in a 4-month-old male Holstein calf.[7,17]

Nowadays, macrolides (tylosin), florfenicol, aminoglycosides (gentamicin and neomycin), lincomycin, and β-lactam antimicrobials (including penicillin and cephalosporins) are commonly used to treat mastitis. In general terms, treatment with antimicrobials is regarded as the main driver of antimicrobial resistance. As a result, resistance to antibiotics used in mastitis is increasing.[18,19] CNS(coagulase-negative Staphylococcus) resistance to erythromycin in the milk of cows with mastitis of 14.3% has been reported.[20] Another study observed the highest percentage of isolates resistant to erythromycin among *S. xylosus* strains from the milk of cows with mastitis.[21] Strains resistant to lincomycin (53%) have also been observed among isolates of *S. xylosus*.[22] Some studies have reported an increase in central nervous system resistance to β-lactam antibiotics, particularly penicillin and ampicillin, which is a worldwide trend.[23,24]

In several studies addressing evolution of resistance, one fearsome fact was observed: bacteria develop cross-resistance against antimicrobial drugs to which they never have been exposed before.[25] Cross-resistance is a severe obstacle for designing effective drug therapies, as it limits possible antibiotic options following unsuccessful drug treatment. Surprisingly, evolution of cross-resistance in *S. xylosus* did not receive much attention until very recently. The ribosomal peptidyl transferase center (PTC) is critical for protein synthesis.[26] Peptidyl transferase reaction involves aminolysis by the α-amino group of the A-site aminoacyl-tRNA of the ester bond that links the nascent peptide to the 3 hydroxyl of the 3 terminal ribose of the P-site tRNA.[27] Many antibiotics that inhibit growth of microorganisms do so by binding to the PTC and inhibiting its activity.[28]

The structural mode of macrolides binding to the entrance of the peptide exit tunnel of the large (50S) ribosomal subunit has been characterized at atomic resolution with X-ray crystallography.[29] Although macrolides bind in the vicinity of the PTC, they do not inhibit peptide bond formation. On the contrary, macrolides block entrance of the nascent chain to the peptide exit tunnel. The study suggested that mutations in ribosomal proteins L4 and L22 in the 50S subunit reduced macrolide susceptibility. Similarly, chloramphenicol, the first broad-spectrum antibiotic, inhibits protein synthesis by targeting the PTC of the bacterial ribosome.[30] Accordingly, macrolides and chloramphenicol share the common mechanism of inhibition of PTC activity in bacteria, and the cross-resistance mechanism of macrolides and chloramphenicol might be related to the PTC.

To better explore mechanism of antibiotic cross-resistance, we introduced site-selective mutations in ribosomal proteins and computational modeling. We propose that in addition to the relationship of ribosomal proteins of cross-resistance, regulation of the protein network may be involved in the mechanism of cross-resistance. In our previous study on tylosin-resistant mechanisms, we suggested that some resistant proteins played an important role.[31] To elucidate the mechanism of resistance evolution of *S. xylosus* against tylosin and florfenicol under selection pressure, we here further explored the aforementioned resistant proteins. We investigated whether distinct mutations in ribosomal proteins were responsible for cross-resistance establishing mutant strains using protein sequencing and computer simulations. Ultimately, quantitative PCR (qPCR) and computer simulations were applied to demonstrate that the resistant proteins were regulated by ribosomal proteins. Our present results demonstrated that mutations in ribosomal proteins were of central importance for the evolution of tylosin and florfenicol cross-resistance.

Methods

Plasmids, Bacterial Strains, Media, and Growth Conditions

Plasmids used in this study are listed in Supplementary Table 1. *S. xylosus* ATCC 700404 was purchased from the American Type Culture Collection (ATCC) and preserved in our lab. All tylosin-resistant *S. xylosus* strains were induced under tylosin pressure in vitro and kept in our lab. All mutants of *S. xylosus* were constructed in this study. The strains in (Supplementary Table 2) were cultured in tryptic soy broth (TSB) at 37°C.

PCR Amplification and DNA Sequencing of Ribosomes in *S. xylosus* and Tylosin-Resistant *S. xylosus*

Based on the genomes of *S. xylosus* and tylosin-resistant *S. xylosus* (tylosin 128 μg/mL), the *rplC, rplD*, and *rplV* fragments were amplified. All primers are listed in Supplementary Table 3. According to a previous describedly method in our lab, the genomes of *S. xylosus* and tylosin-resistant *S. xylosus* were extracted. We chosen the PrimeStar GXL DNA polymerase to amplify the fragments of *rplC*, *rplD*, and *rplV*. Then, the PCR products were visualized by agarose gel electrophoresis. DNA sequences of PCR products were tested at Comate Bioscience. Subsequently, the Dnaman software was used to compare amino acid (nucleotide) sequences of *S. xylosus* with tylosin-resistant *S. xylosus*.

Construction of the Mutant *S. xylosus*

The recombinant shuttle plasmids (PBT2-rplC, PBT2-rplD, and PBT2-rplV) were used according to a protocol in our lab with some modifications.[32] Upstream and downstream fragments of *rplC*, *rplD*, and ***rplV* gene**s were amplified from the genomic DNA of *S. xylosus*. The gfp gene and mutant fragments of *rplC*, *rplD* and rplV were obtained from plasmids, including gfp-T, mutant rplC-T, rplD-T, and rplV-T. Then, in determinate order, the above PCR products were linked by overlap PCR and cloned to pClone007 blunt simple vector. The constructed plasmids were named based on mutant sites as pClone007-rplC, pClone007-rplD, and pClone007-rplV. Next, the constructed plasmids were digested and cloned using the restriction sites of the *E. coli–Staphylococcus* shuttle vector pBT2, and thus the recombinant shuttle plasmids PBT2-rplC, PBT2-rplD, and PBT2-rplV were obtained. The primers and restriction sites used in this section are listed in Supplementary Table 4

The mutant strains were created using a previously described protocol with some modifications.[33] The recombinant shuttle plasmids were introduced into *S. xylosus* by electroporation. The strains with recombinant shuttle plasmids were grown in tryptic soy broth at 37°C for 24 hours, then transferred to fresh medium at 42°C for another 24 hours, which was identified as one passage. Based on the *gfp* gene, flow cytometry (FC) was used to detect the mutant strains of seven, nine, and eleven passages. The blank strains without recombinant shuttle plasmids served as controls. The mutant strains screened by FC were identified by PCR amplification and sequences of mutant fragments (Supplementary Figure 1). Finally, the mutant strains were named L3 (*rplC*) N135G, A137G, S142A and R162K mutant *S. xylosus*, L4 (*rplD*) S158N and A164E mutant *S. xylosus*, and L22 (*rplV*) 97KRTSAIN98 insertion mutant *S. xylosus*.

Evaluation of Mutant *S. xylosus* Susceptibility

Minimum inhibitory concentration (MIC) assays of tylosin and florfenicol to *S. xylosus* and mutant *S. xylosus* were done as previously reported.[34] Briefly, *S. xylosus* and mutant strains were grown overnight at 37°C. The overnight cultures were diluted in sterile physiological saline, which corresponded to 108 colony-forming units/mL. Then, the cultures were diluted again with TSB to 106 colony-forming units/mL. Finally, 100 mL samples were added to the 96-well plate containing serial dilutions of tylosin in culture medium. Control bacterial and medium were cultivated in the absence of tylosin. The MIC was defined as the lowest concentration of inhibitor to visually inhibit growth. The assays were repeated three times.

MD Simulation

We employed MD simulations for *S. xylosus* 23S rRNA, L22, and L22 97KRTSAIN98 insertion mutants to obtain corresponding three-dimensional structures and studied the functional changes in the structure. All MD simulations were performed using Gromacs 2018.[35] All systems were solvated in a cubic water box with 12 Å buffer distance between the solvent box wall and the nearest solute atoms and neutralized by addition of 150 mM Na^+ or Cl^- ions. The Amber99SB-ILDN force field was assigned to the RNA, protein, and ions.[36] Water was modeled using the TIP3P water model. All structure models were first minimized to relax the solvent and optimize the system using steepest descent. Then, a short 100 ps NVT preequilibration simulation was performed whereby the heavy atoms of RNA or protein were positionally restrained using a force constant of 200 kJ/(mol•nm). Finally, the production run 23S rRNA and L22 were positionally restrained to the backbone of ribose (C1' atom), phosphate (P atom), and Cα atom and a positional force constant of 200

kJ/(mol•nm) was applied. L22 and L22 97KRTSAIN98 insertion mutant production runs were performed without any positional constraints. The temperature of simulations was controlled using the Nosé–Hoover thermostat and the pressure was held at 1 bar using an isotropic coupling with the Parrinello–Rahman barostat. Long-range electrostatic interactions were calculated using the particle mesh Ewald method with a real-space cutoff value of 1.2 nm. Unbonded interactions were cut off at 1.2 nm.

Docking

The docking of antibiotics to the receptor was performed using Glide.[37] Tylosin and florfenicol were produced in Schrödinger Maestro software. The LigPrep module in the software was introduced for geometric optimization using the OPLS_2005 force field. The receptor models were prepared in the software under the OPLS_2005 force field. Hydrogen atoms were added according to the physiological pH (7.5) with the Propka tool in Maestro Protein Preparation Wizard to optimize the hydrogen-bond network. Constrained energy minimization was conducted on the fully atomic models. Cubic boxes were centered on the tylosin and florfenicol mass center with a radius of 12 Å for the peptide exit tunnel and PTC of receptor.

Investigation of Resistant Gene Expression in the Evolution of Tylosin-Resistant *S. xylosus*

Here, five genes related to resistance were investigated (16s rRNA was used as an internal control). The primers of target genes are listed in Supplementary Table 5. Total RNA of different levels of tylosin-resistant *S. xylosus* was extracted as specified by manufacturer, including tylosin (8 μg/mL, 32 μg/mL, and 128 μg/mL). Next, an equivalent amount of total DNA-free RNA from the last sample was reverse-transcribed using a PrimEScript RT reagent kit with gDNA Eraser. Finally, real-time PCR was run for 40 cycles (95°C for 15 s, 60°C for 35 s) after initial 30 s incubation at 95°C. The assays were repeated three times.

Investigation of Resistant Gene Expression in Mutant *S. xylosus*

Five genes related to resistance were investigated at mRNA level, and 16S rRNA was used as an internal control. The list of primers is shown in Supplementary Table 5. Total RNA of *S. xylosus* and mutant *S. xylosus* was extracted. Then, the equivalent amount of total DNA-free RNA from the last sample was reverse-transcribed using PrimeScript kit with gDNA Eraser. Real-time PCR reactions were run for 40 cycles (95°C for 15 s, 60°C for 35 s) after initial 30 s incubation at 95°C. The assays were repeated three times.

Statistical Analysis

All MIC values were determined in triplicate to ensure reliability. Data on real-time PCR were analyzed (and figures drawn) using GraphPad Prism. Dnaman and BLAST were used to identify DNA sequences. Values are expressed as means ± SD. Statistical differences among the groups were compared by one-way ANOVA, and significant means were separated using Tukey's honestly significant difference at $p<0.05$.

Results and Discussion

Mutations in Ribosomal Proteins of Tylosin-Resistant *S. xylosus*

To probe the molecular evolution of tylosin-resistant *S. xylosus*, we sequenced PCR-amplified DNA of ribosomal proteins L3, L4, and L22 from *S. xylosus* and tylosin-resistant *S. xylosus*. Sequencing revealed mutations N135G, A137G, S142A and R162K in *rplC* (ribosomal protein L3), S158N and A164E in *rplD* (ribosomal protein L4), and 97KRTSAIN98 insertion in *rplV* (ribosomal protein L22.) The L3 loop F127–P170 locates in the vicinity of PTC, and deletions or mutations in the loop may reshape the drug-binding pocket, hindering antibiotic binding of *S. aureus*.[38] The mutations of L3 found in our present study were consistent with results of the previous study. Hence, we concluded that mutations N135G, A137G, S142A and R162K in L3 were involved in the molecular evolution of cross-resistance. In addition, the L4 W65–Q75 loop locates in the vicinity of the phosphate of ribosomal RNA A2059, which belongs to the

multidrug-binding pocket, and mutations in the W65–Q75 loop might affect the conformation of A2059 leading to multidrug resistance [34]. However, the mutations of L4 found in our present study were not in line with the region mentioned before. In addition, the mutations, deletions, and insertions in the L22 hairpin loop, which were part of the exit tunnel R80-S108, would confer resistance to erythromycin, synercid and telithromycin in multidrug-resistant *S. aureus*.[39,40] Hence, it is reasonable that 97KRTSAIN98 insertion in L22 was involved in the molecular evolution of cross-resistance.

Identification of Mutant *S. xylosus*

Our protein sequence analysis point out that mutations of ribosomal proteins L3 (*rplC*), L4 (*rplD*) and L22 (*rplV*) may relate to tylosin resistance of *S. xylosus*. As such, a ribosomal mutant *S. xylosus* was constructed, and the *gfp* gene instead of resistance genes as screening flags was used to find mutant strains, since our aim was to clarify the drug-resistant mechanism, and resistance genes would disturb the results. Then, FC was used to detect mutant strains on the basis of the fluorescence of the expressed *gfp* gene. Compared with the wild-type strain, the screened strains showed strong fluorescence, and fluorescence intensity continually increased along with screening generations (Figure 1). The screened strains were further identified by PCR amplification and sequencing (Supplementary Figure 2). As expected, the sequencing results of the amplified fragments were in accord with the introduced mutant sites.

Determination of Mutant *S. xylosus* Susceptibility

Next, we carried out MIC assays to seek mutant sites thatwere related to the molecular evolution mechanism of tylosin resistance. The resistance to tylosin increased from 0.5 μg/mL in wild-type *S. xylosus* to 128 μg/mL in the L22 (*rplV*) mutant. An additional interesting result was that the MIC against florfenicol increased from 0.5 μg/mL in wild-type *S. xylosus* to 2 μg/mL in L22 (*rplV*) mutant. In contrast, the resistance to tylosin and florfenicol did not change for L3 (*rplC*) or L4 (*rplD*) mutants compared to wild-type *S. xylosus*.

Structure of Tylosin and Florfenicol Bound to the Large Ribosomal Subunit of *S. xylosus*

Crystal structures of the ribosomal subunit from *S. xylosus* in the absence or presence of bound antibiotic and *S. xylosus*–antibiotic complex have not been reported yet, making it difficult to understand the structural relationship between *S. xylosus* and the two antibiotics (tylosin and florfenicol). Fortunately, co-crystal structure of tylosin bound to the related 50S ribosomal subunit of *Haloarcula marismortui* has been resolved. This study revealed tylosin bound in a narrow part of the ribosomal peptide exit tunnel at a site that lies between the PTC and the constriction in the tunnel near protein L22.[41] The crystal structure of the 50S ribosomal subunit complexed with the clinically relevant antibiotic chloramphenicol, with a closely related chemical structure to florfenicol, showed that the antibiotic-binding site was composed exclusively of segments of 23S ribosomal RNA at the entrance to the peptide exit tunnel or the peptidyl transferase

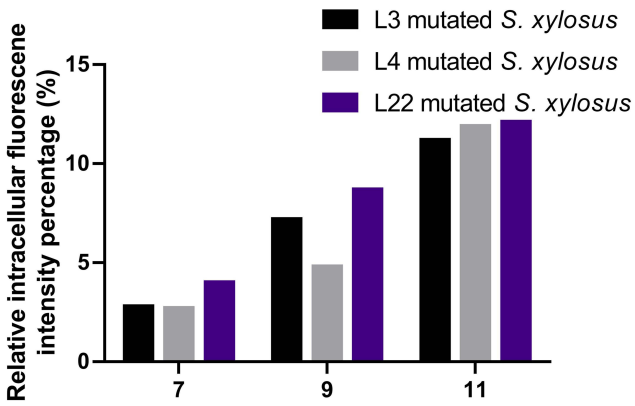

Figure 1 In order to screen the mutant strains, we used flow cytometry to measure the fluorescence of GFP in mutated *S. xylosus*, after seven, nine, and eleven generations.

cavity.[42] Based on these studies, we suggested that tylosin and florfenicol contact primarily the peptide exit tunnel or PTC of 23S rRNA of *S. xylosus* and the mycinose moiety of tylosin binds L22.

We used computational methods to construct a three-dimensional structure of 23S rRNA and L22 of *S. xylosus* and then docked antibiotics to the structure to elucidate the structural basis of ribosome–antibiotic interactions. We used a fully automatic procedure with Swiss-Model[43] to model L22 of *S. xylosus* based on a related homologous L22 from *S. aureus* (PDB ID: 4WCE)[38] that shared 96% sequence identity. The homology model of *S. xylosus* L22 shared a common overall structure of L22 from other species.[38,41] It consisted of a globular domain with three α-helices and an extended loop with two- or three-stranded antiparallel β-sheets forming a β-hairpin, which extended approximately 30 Å from the globular domain (Figure 2A and B). Because homology modeling of RNA remains a challenge,[44] a more effective method to build *S. xylosus* 23S rRNA was implemented. We found that the sequence alignment of the 23S rRNA of 50S nucleotides showed 93% identity with only 97 different bases between *S. xylosus* and *S. aureus* (Supplementary Figure 3). For high sequence conservation, we directly mutated these local bases in the crystal structure of *S. aureus* 23S rRNA to build the initial three-dimensional structure for *S. xylosus* 23S rRNA. Then, we combined the homology model of L22 and the mutant 23S rRNA into a new *S. xylosus* model. The interactions between bases and sidechains of amino acids, and those between side chains of amino acids in this new model were recalibrated by performing MD simulations which provided a more reasonable *S. xylosus* structure (Figure 2C). The MD trajectory showed that RMSD of 23S rRNA and L22 within 1.4 Å during 5 ns simulation (Supplementary Figure 4), suggesting that the molecular interactions in this new *S. xylosus* mode were stable.

Then, we extracted the last configuration from the simulation trajectory as a starter to obtain a *S. xylosus*–antibiotic complex model. As indicated in Figure 3, *S. xylosus* ribosomal subunit complexed with tylosin shows that the saccharide

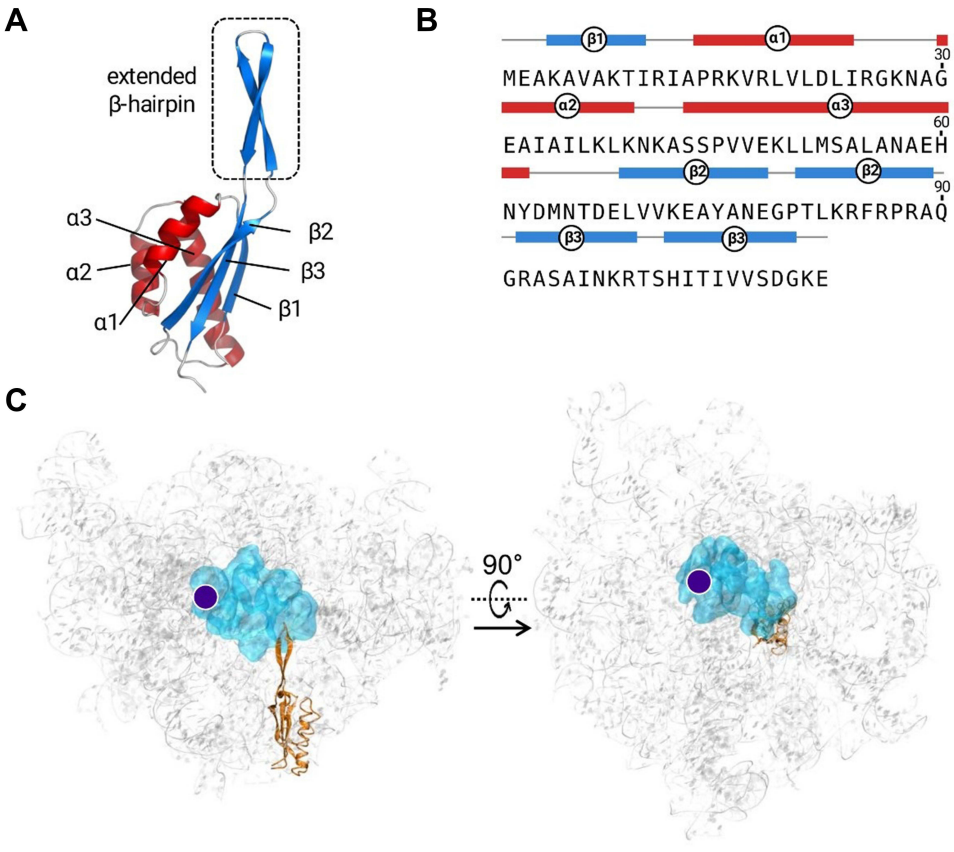

Figure 2 (**A**) 3D model of *S. xylosus* L22. The overall structure consists of three α-helices and three β-strands. The encircled box indicates the location of β-hairpin. (**B**) The amino acid sequence of L22 together with distribution of particular secondary structures. (**C**) The overall structure of *S. xylosus* ribosomal subunit. The 23S rRNA is shown in gray, the L22 is shown in orange, the antibiotic-binding site is shown in cyan, and the PTC location is marked as a purple dot.

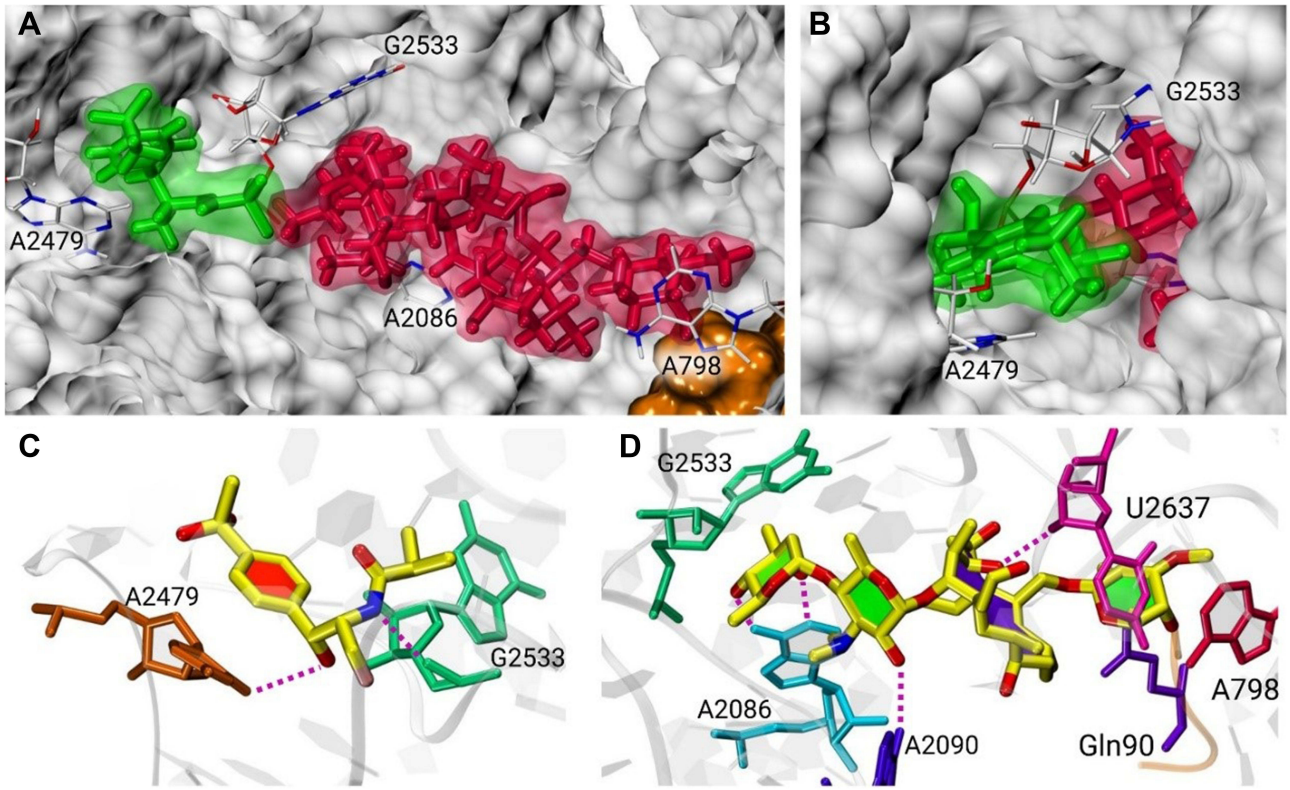

Figure 3 A model of antibiotics in complex with the *S. xylosus* ribosome. (**A**) Superposition of the binding locations of tylosin (red) and florfenicol (green). Surface representation of the structure of 23S rRNA (cyan) and L22 (orange). Tylosin binds to the peptide exit tunnel, whereas florfenicol is above the exit tunnel of PTC peptide (**B**). The hydrogen bond interactions (purple dash) of florfenicol (**C**) and tylosin (**D**) with 23S rRNA in the ribosome.

branch linked to lactone ring C5 contacts with the PTC and the mycinose linked to C14 that points to the exit tunnel consisting of L22 and domain II of 23S rRNA. It was similar to the binding orientation in other ribosome–tylosin complexes elsewhere.[41] The tylosin-binding sites include nucleotides A798 (A748, E. coli), A2086 (A2041, E. coli), A2090 (A2045, E. coli), G2533 (G2508, E. coli), U2637 (U2575, E. coli) and L22 Gln90, which establish either hydrophobic or hydrogen bond interactions with ligands. In the model of *S. xylosus*-florfenicol, florfenicol was bound at the PTC with the OH– and the NH groups forming hydrogen bonds with A2479 (A2454, *E. coli*) and A2533 (A2508, E. coli). These results clearly illustrate that tylosin is bound at the polypeptide exit tunnel, which may inhibit translation by blocking the egress of nascent polypeptides. In contrast, the florfenicol-binding site is located at the A-site and may block PTC activity by hampering the binding of transfer RNA to the A-site.

Structural Analysis of L22 Resistance Mechanism

The resistance to tylosin increased from 0.5 μg/mL in wild-type *S. xylosus* to 128 μg/mL in L22 (*rplV*) mutant (97KRTSAIN98 insertion). Previous research showed that the point mutations, deletions, and insertions in the uL22 hairpin loop that is part of the exit tunnel wall in residues R80–S108 would confer resistance to erythromycin, synercid, and telithromycin in multidrug-resistant *S. aureus*.[39,40] Along similar lines, resistance mutations were also observed in additional bacterial species, such as *Legionella pneumophila*.[45] Hence, it is reasonable to infer that 97KRTSAIN98 insertion in L22(*rplV*) was involved in the molecular evolution mechanism of cross-resistance. In order to illustrate the above result, the effect of the mutations identified on the L22 structure was investigated by both molecular modeling and MD simulations. According to the modeled structures, the mutated site of L22 (*rplV*) was located in the β-hairpin of the wild-type L22 (Supplementary Figure 5). Therefore, it could potentially destroy the hairpin secondary structure. Considering the flexibility of protein that ruled function and controlled activity, we further investigated the structure and motion of wild-type as well as mutant L22 using MD simulations. As shown in Figure 4A, the L22 protein

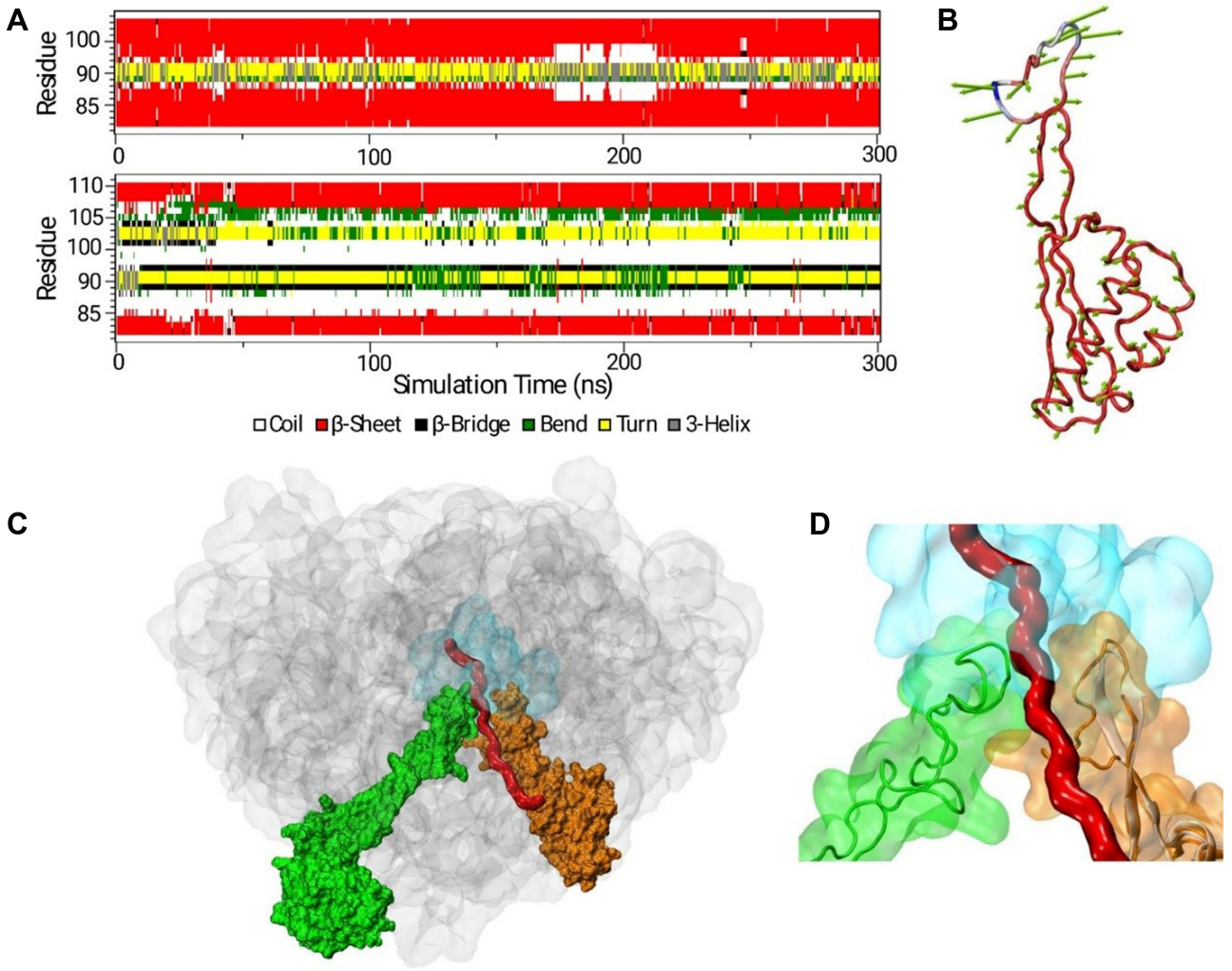

Figure 4 L22 resistance mechanism. (**A**) Secondary structure changes of the L22 β-hairpin during MD simulations in the wild type (upper panel) and 97KRTSAIN98 insertion mutant (lower panel). (**B**) Intrinsic mobility of the L22 mutant calculated from PCA analysis. The lengths of the green vectors scale with the domain motions. (**C** and **D**) Structure of the nascent polypeptide in the exit tunnel. The model of the nascent polypeptide chain is shown in red. The structure of the ribosome shown comprises the 23S rRNA and the homology model of L4 and L22 mutants. The 23S rRNA is shown in gray, the antibiotic-binding site in cyan, L4 in green, and L22 in orange. Wild-type L22 is represented as a white cartoon (**D**).

extended β-hairpin remained stable in a folded-sheet structure in the wild type. In contrast, the mutant protein in this region became highly flexible and disordered, supporting mutant-induced β-hairpin disruption in L22 (*rplV*). We used principal component analysis (PCA)[46] to calculate the protein backbone motion in the MD trajectory. This analysis revealed that the mutant insertion residues were unstructured and underwent large changes, breaking the β-hairpin formation (Figure 4B). The docking study indicated that the tylosin-binding site interacted with the mycinose moiety with the L22 β-hairpin. An apparent disruption of the conformation of the extended β-hairpin might directly influence tylosin binding. In addition, this hairpin contributed to the formation of part of the ribosomal tunnel wall for the exit of the nascent peptide (Figure 4C and D) along with 23S rRNA and ribosomal protein L22. The L22 mutant could change the surface properties or perturb the three-dimensional structure of the tunnel wall. Therefore, it might influence translation by regulating the exit of nascent peptides. Taken together, the L22 (*rplV*) 97KRTSAIN98 insertion mutant has double effects on the tylosin resistance. (1) Breaking the interaction of the tylosin mycinose moiety with the L22 β-hairpin. (2) Altering the structure of the exit tunnel wall. In contrast, as no direct contact was found between L22 and florfenicol, the resistance most likely occurs indirectly via perturbation of the exit tunnel wall. Therefore, the MIC of mutant strains against florfenicol did not return to the level of resistant strains (0.5 μg/mL to 2 μg/mLin L22 (*rplV*) mutant).

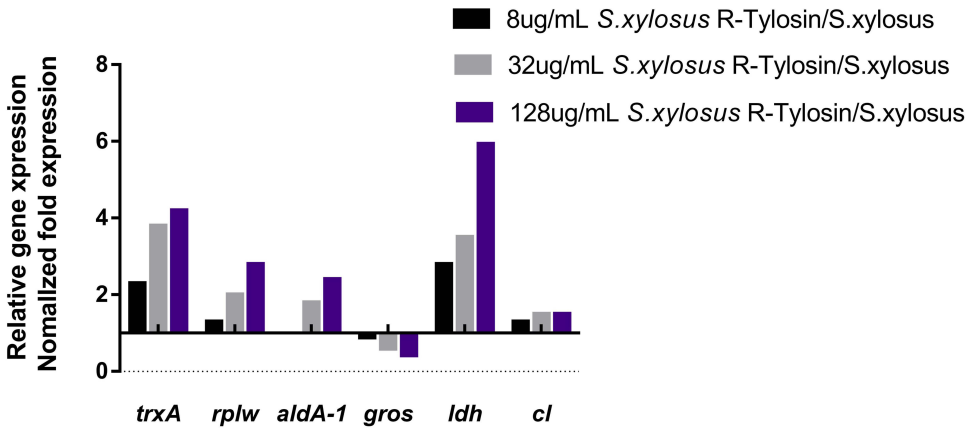

Figure 5 Changes in resistant proteins at mRNA level of different tylosin-resistance levels in *S. xylosus*, including thioredoxin (*trxA*), 50S ribosomal protein L23 (*rplW*), aldehyde dehydrgenase (*aldA-1*), chaperonin (*gros*), L-lactic dehydrogenase (*ldh*), and chloramphenicol-resistant protein (*cl*).

To further investigate the role of mutations in L3 and L4, we constructed three-dimensional structures of L3 and L3 (*rplC*) mutant, and L4 and L4 (*rplD*) mutant based on homologous structure from *S. aureus* (PDB ID: 4WCE), which shares 90% sequence identity. Comparing these modeled structures, no structural difference between wild-type and mutant was evident (Supplementary Figure 6A and B). In particular, none of the mutated amino acids in the modeled structures was adjacent to the tylosin- and florfenicol-binding pockets or to the exit tunnel of nascent peptide (Supplementary Figure 6C), indicating that these mutations do not alter the binding of these two antibiotics and disrupt the progression of the nascent peptide.

Identification of Resistant Gene Expression in Evolution of Tylosin-Resistant *S. xylosus* and L22 Mutant *S. xylosus*

Antibiotic resistance might not only depend on mutations in ribosomal proteins but might also be influenced by the interaction protein network.[47] Our previous study showed that proteins related to stress-response and transcription in the tylosin resistant *S. xylosus* markedly changed at mRNA level. We concluded that during the evolution of tylosin and florfenicol resistance, expression of the above resistant proteins may change at mRNA level. In order to identify the relationship of the resistant proteins to the evolution of tylosin-resistance in *S. xylosus*, the involved proteins have been probed at the mRNA level. As shown in Figure 5, the mRNA level of *rplW* (50S ribosomal protein L23), *aldA* (aldehyde dehydrogenase), *trxA* (thioredoxin), *gro*s (chaperonin) gradually increased during the evolution of tylosin-resistance in *S. xylosus* while the mRNA level of *ldh* (lactate dehydrogenase) was reduced. These results confirmed the influence of the corresponding proteins on the evolution of tylosin resistance in *S. xylosus*.

To explore the relationship of mutations in the ribosomal proteins for the development of tylosin-resistance in *S. xylosus* further, we determined the mRNA level of resistant proteins in the L22 mutant of *S. xylosus*. The results (Figure 6) showed that the mRNA level of the resistant proteins, including thioredoxin (*trxA*), 50S ribosomal protein L23 (*rplW*), aldehyde dehydrgenase (*aldA-1*), chaperonin (*gros*), L-lactic dehydrogenase (*ldh*) and chloramphenicol resistant protein (*cl*) in the L22 mutant strain changed significantly, demonstrating that the resistant proteins were regulated by ribosomal protein L22.

Conclusion

In summary, our study strongly suggested that tylosin-resistant *S. xylosus* cross-resistance to florfenicol was related to ribosomal protein L22. Computational analysis fostered this proposition, revealing atomic details for the action of the two antibiotics (Figure 7): Tylosin was bound to the ribosomal polypeptide exit tunnel adjacent to the PTC, whereas florfenicol was bound to the PTC blocking A-site. The evolution of increasing resistance of *S. xylosus* against tylosin and florfenicol was related to the interaction protein network, which included thioredoxin *(trxA*), 50S ribosomal protein L23

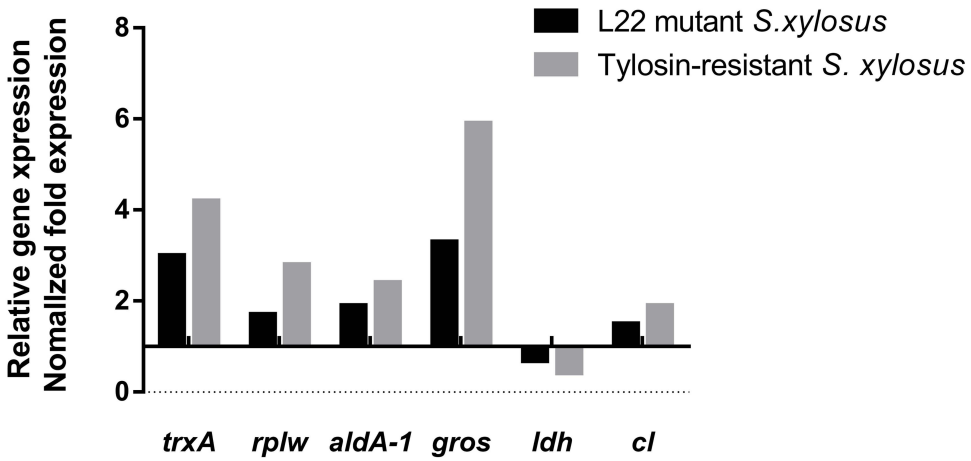

Figure 6 Changes in resistant proteins at mRNA level of L22 (*rplV*) mutant *S. xylosus*, including thioredoxin (*trxA*), 50S ribosomal protein L23 (*rplW*), aldehyde dehydrgenase (*aldA-1*), chaperonin (*gros*), L-lactic dehydrogenase (*ldh*), and chloramphenicol-resistant protein (*cl*).

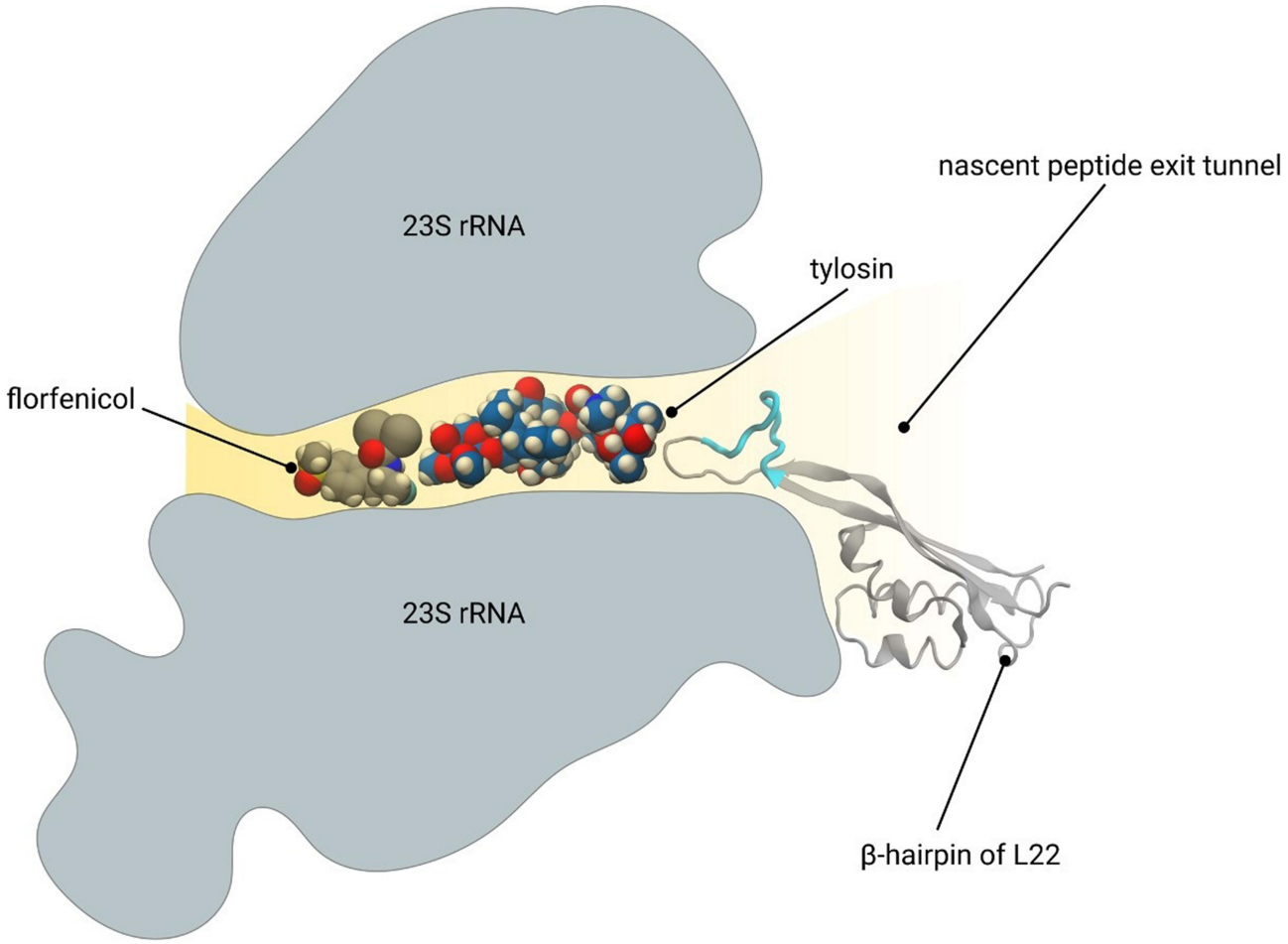

Figure 7 The drug-resistance mechanism of tylosin and florfenicol. Florfenicol (gray and red spheres) binds to the deep narrow pocket of the nascent peptide exit tunnel, which is far away from the β-hairpin of L22. A loop (in cyan) inserted into the β-hairpin of L22 has limited influence on the drug resistance of florfenicol. Tylosin (blue and red spheres), which is much larger than florfenicol, binds to the entrance of the nascent peptide exit tunnel. It closes into the β-hairpin of L22. The insertion of additional amino acid (in cyan) shows great impact on the drug resistance of tylosin.

(*rplW*), aldehyde dehydrgenase (*aldA-1*), chaperonin (*gros*), L-lactic dehydrogenase (*ldh*) and chloramphenicol-resistant protein (*cl*). Our work provides insightful views into the molecular mechanism of *S. xylosus* resistance that could be useful for the development of next-generation antibiotics.

Acknowledgments

We appreciate financial support from the Science and Technology Foundation of Guizhou Province through the Qianke He Foundation (ZK[2021]General 083). The work of Yanhua Li was supported by China Agriculture Research System and National Key Research and Development Program of China (2018YFD0500300) and National Nature Science Foundation of China (31772787). The work of Shuguang Yuan was supported by funding from Chinese Academy of Sciences Shenzhen Institutes of Advanced Technology (JCYJ20200109114818703) and Guangdong Province (2019QN01Y306).

Disclosure

The authors declare no competing interests.

References

1. Wilson DN, Hauryliuk V, Atkinson GC, O'Neill AJ. Target protection as a key antibiotic resistance mechanism. *Nat Rev Microbiol*. 2020;18(11):1–12. doi:10.1038/s41579-020-0386-z
2. Fan L, Xiao HP. 范琳, 肖和平. 世界卫生组织发布的耐药结核病指南带来的思考与挑战[J]. 中华结核和呼吸杂志 [The thinking and challenge from the drug-resistant tuberculosis guidelines by World Health Organization]. *Zhonghua jie he he hu xi za zhi*. 2018;41(1):3–5. [Chinese]. doi:10.3760/cma.j.issn.1001-0939.2018.01.003
3. Tangcharoensathien V, Sattayawutthipong W, Kanjanapimai S, Kanpravidth W, Brown R, Sommanustweechai A. Antimicrobial resistance: from global agenda to national strategic plan, Thailand. *Bull World Health Organ*. 2017;95(8):599–603. doi:10.2471/BLT.16.179648
4. Charmpi C, Veken DVD, Reckem EV, Vuyst LD, Leroy F. Raw meat quality and salt levels affect the bacterial species diversity and community dynamics during the fermentation of pork mince. *Food Microbiol*. 2020;89:103434. doi:10.1016/j.fm.2020.103434
5. Visscher AD, Piepers S, Haesebrouck F, Supre K, Vliegher SD. Coagulase-negative Staphylococcus species in bulk milk: prevalence, distribution, and associated subgroup- and species-specific risk factors. *J Dairy Sci*. 2017;100(1):629–642. doi:10.3168/jds.2016-11476
6. Wang D, Zhao L, Su R, Jin Y. Effects of different starter culture combinations on microbial counts and physico-chemical properties in dry fermented mutton sausages. *Food Sci Nutr*. 2019;7(6):1957–1968. doi:10.1002/fsn3.989
7. Rissi DR, Elsmo EJ, Sanchez S. Cystitis and peritonitis caused by Staphylococcus xylosus infection in a calf. *Braz J Vet Pathol*. 2015;8:99–101.
8. Giordano N, Corallo C, Miracco C, et al. Erythema nodosum associated with Staphylococcus xylosus septicemia. *J Microbiol Immunol Infect*. 2016;49(1):134–137. doi:10.1016/j.jmii.2012.10.003
9. Jabbar H, Al-Mathkhury F, Flaih MT, Khalil H. Histopathological effects of S. xylosus peptidoglycan in comparison to E. coli lipopolysaccharide in the urinary tract of mice. *Turk J Med Sci*. 2014;42(1):1278–1285.
10. Seif SS, El-Rehewy MS, Ghazaly MM, Abd-Elhamid MH. Biofilm formation by blood stream staphylococcal isolates from febrile pediatric cancer patients at south Egypt cancer institute. *J Am Sci*. 2011;7(1):674–686.
11. Omran AS, Hussein AN. Molecular investigation of mecgene among coagulase negative Staphylococcus isolated from different cases. *J Phys Conf Ser*. 2019;1234:012074.
12. Wang J, Qu Q, Liu X, Cui W, Li Y. 1-Hydroxyanthraquinone exhibited antibacterial activity by regulating glutamine synthetase of Staphylococcus xylosus as a virulence factor. *Biomed Pharmacother*. 2020;123:109779. doi:10.1016/j.biopha.2019.109779
13. Macfadyen AC, Leroy S, Harrison EM, Parkhill J, Paterson GK, Paterson GK. Staphylococcus pseudoxylosus sp. nov., isolated from bovine mastitis. *Int J Syst Evol Microbiol*. 2019;69:8. doi:10.1099/ijsem.0.003416
14. Klibi A, Jouini A, Andolsi RBE, Kmiha S, Maaroufi A. Epidemiology of β -lactamase-producing staphylococci and gram negative bacteria as cause of clinical bovine mastitis in Tunisia. *Biomed Res Int*. 2019;2019:1–9. doi:10.1155/2019/2165316
15. Ndahetuye JB, Persson Y, Nyman AK, Tukei M, Ongol MP, Bge R. Aetiology and prevalence of subclinical mastitis in dairy herds in peri-urban areas of Kigali in Rwanda. *Springer Open Choice*. 2019;51(7):2037–2044.
16. De Almeida CC, Pizauro LJL, Soltes GA, et al. Some coagulase negative Staphylococcus spp. isolated from Buffalo can be misidentified as Staphylococcus aureus by phenotypic and Sa442 PCR methods. *BMC Res Notes*. 2018;11:1. doi:10.1186/s13104-018-3449-8
17. Russo M, Invernizzi A, Gobbi A, Radaelli E. Diffuse scaling dermatitis in an athymic nude mouse. *Vet Pathol*. 2013;50(4):722–726. doi:10.1177/0300985812463408
18. Baqer BAA, Mahdi LH. Biofilm formation and antibiotic resistance of coagulase-negative staphylococci isolated from lactating women with mastitis in Baghdad, Iraq. *Indian J Public Health Res Dev*. 2019;10(10):2175. doi:10.5958/0976-5506.2019.03175.9
19. Claudia G, Bonetto CC, Vissio C, et al. Prevalence and antibiotic susceptibility of coagulase-negative Staphylococcus species from bovine subclinical mastitis in dairy herds in the central region of Argentina - ScienceDirect. *Revista Argentina de Microbiología*. 2016;48(1):50–56. doi:10.1016/j.ram.2015.12.001
20. Lüthje P, Schwarz S. Antimicrobial resistance of coagulase-negative staphylococci from bovine subclinical mastitis with particular reference to macrolide-lincosamide resistance phenotypes and genotypes. *J Antimicrob Chemoth*. 2006;57(5):966–969. doi:10.1093/jac/dkl061
21. Kot B, Piechota M, Antos-Bielska M, et al. Antimicrobial resistance and genotypes of staphylococci from bovine milk and the cowshed environment. *Pol J Vet Sci*. 2012;15(4):741–749. doi:10.2478/v10181-012-0113-4

22. Resch M, Nagel V, Hertel C. Antibiotic resistance of coagulase-negative staphylococci associated with food and used in starter cultures. *Int J Food Microbiol*. 2008;127(1–2):99–104. doi:10.1016/j.ijfoodmicro.2008.06.013
23. Botrel MA, Haenni M, Morignat E, Sulpice P, Madec JY, Calavas D. Distribution and antimicrobial resistance of clinical and subclinical mastitis pathogens in dairy cows in Rhone-Alpes, France. *Foodborne Pathog Dis*. 2010;7(5):479–487. doi:10.1089/fpd.2009.0425
24. Piessens V, Coillie EV, Verbist B, et al. Distribution of coagulase-negative Staphylococcus species from milk and environment of dairy cows differs between herds. *J Dairy Sci*. 2011;94(6):2933–2944. doi:10.3168/jds.2010-3956
25. Dean Z. Antibiotic interactions, collateral sensitivity, and the evolution of multidrug resistance in E. faecalis; 2019.
26. Klinge S, Woolford JL. Ribosome assembly coming into focus. *Nat Rev Mol Cell Biol*. 2018;20(2):116–134.
27. Hansen JL, Moore PB, Steitz TA. Structures of five antibiotics bound at the peptidyl transferase center of the large ribosomal subunit. In: *Structural Insights into Gene Expression and Protein Synthesis*. World Scientific Pub Co Inc; 2020.
28. Ea S, Flemmich L, Ds K, Ns VL, Micura R, Ys P. Structural basis for the context-specific action of classic peptidyl transferase inhibitors. *Cold Spring Harbor Lab*. 2021;29:152–161.
29. Martin L, Nilsson K, Lukk E, et al. Erythromycin resistance by L4/L22 mutations and resistance masking by drug efflux pump deficiency. *EMBO J*. 2009;28(6):736–744. doi:10.1038/emboj.2009.17
30. Syroegin EA, Flemmich L, Klepacki DS, Vazquez-Laslop NS, Polikanov YS. Structural basis for the context-specific action of classic peptidyl transferase inhibitors; 2021.
31. Liu X, Wang J, Chen M, Che R, Li Y. Comparative proteomic analysis reveals drug resistance of Staphylococcus xylosus ATCC700404 under tylosin stress. *BMC Vet Res*. 2019;15(1). doi:10.1186/s12917-019-1959-9
32. Zhou YH, Xu CG, Yang YB, et al. Histidine metabolism and IGPD play a key role in cefquinome inhibiting biofilm formation of Staphylococcus xylosus. *Front Microbiol*. 2018;9:665. doi:10.3389/fmicb.2018.00665
33. Brückner R. Gene replacement in Staphylococcus carnosus and Staphylococcus xylosus. *FEMS Microbiol Lett*. 2010;151(1):1–8. doi:10.1111/j.1574-6968.1997.tb10387.x
34. Xu CG, Yang YB, Zhou YH, et al. Comparative proteomic analysis provides insight into the key proteins as possible targets involved in aspirin inhibiting biofilm formation of Staphylococcus xylosus. *Front Pharmacol*. 2017;8:543. doi:10.3389/fphar.2017.00543
35. Abraham MJ, Murtola T, Schulz R, et al. GROMACS: high performance molecular simulations through multi-level parallelism from laptops to supercomputers. *SoftwareX*. 2015;1:19–25. doi:10.1016/j.softx.2015.06.001
36. Lindorff-Larsen K, Piana S, Palmo K, et al. Improved side-chain torsion potentials for the Amber ff99SB protein force field. *Proteins*. 2010;78(8):1950–1958. doi:10.1002/prot.22711
37. Friesner RA, Murphy RB, Repasky MP, et al. Extra precision glide: docking and scoring incorporating a model of hydrophobic enclosure for protein-ligand complexes. *J Med Chem*. 2006;49(21):6177–6196. doi:10.1021/jm051256o
38. Eyal Z, Matzov D, Krupkin M, et al. Structural insights into species-specific features of the ribosome from the pathogen Staphylococcus aureus. *Proc Natl Acad Sci U S A*. 2015;112(43):E5805–14. doi:10.1073/pnas.1517952112
39. Gentry D, Holmes D. Selection for high-level telithromycin resistance in Staphylococcus aureus yields mutants resulting from an rplB-to-rplV gene conversion-like event. *Antimicrob Agents Chemother*. 2008;52(3):1156–1158. doi:10.1128/AAC.00923-07
40. Brigitte M, Annie C, Bülent B, et al. Resistance to quinupristin-dalfopristin due to mutation of L22 ribosomal protein in Staphylococcus aureus. *Antimicrob Agents Chemother*. 2002;46(7):2200. doi:10.1128/AAC.46.7.2200-2207.2002
41. Hansen JL, Ippolito JA, Ban N, Nissen P, Moore PB, Steitz TA. The structures of four macrolide antibiotics bound to the large ribosomal subunit. *Mol Cell*. 2002;10(1):117–128. doi:10.1016/s1097-2765(02)00570-1
42. Vázquez-Laslop N, Mankin AS. How macrolide antibiotics work. *Trends Biochem Sci*. 2018;43(9):668–684. doi:10.1016/j.tibs.2018.06.011
43. Waterhouse A, Bertoni M, Bienert S, et al. Swiss-MODEL: homology modelling of protein structures and complexes. *Nucleic Acids Res*. 2018;46(W1):W296–W303. doi:10.1093/nar/gky427
44. Šponer J, Bussi G, Krepl M, et al. RNA structural dynamics as captured by molecular simulations: a comprehensive overview. *Chem Rev*. 2018;118(8):4177–4338. doi:10.1021/acs.chemrev.7b00427
45. Descours G, Ginevra C, Jacotin N, et al. Ribosomal mutations conferring macrolide resistance in legionella pneumophila. *Antimicrob Agents Chemother*. 2017;61(3):e02188–16. doi:10.1128/AAC.02188-16
46. Bakan A, Meireles LM, Bahar I. ProDy: protein dynamics inferred from theory and experiments. *Bioinformatics*. 2011;27(11):1575–1577. doi:10.1093/bioinformatics/btr168
47. Kohanski MA, Dwyer DJ, Collins JJ. How antibiotics kill bacteria: from targets to networks. *Nat Rev Microbiol*. 2010;8(6):423–435. doi:10.1038/nrmicro2333